Available online at www.sciencedirect.com
SCIENCE DIRECT®
Journal of Sound and Vibration 273 (2004) 1–32
JOURNAL OF SOUND AND VIBRATION
www.elsevier.com/locate/jsvi

Transient seismic wave propagation in a multilayered cracked geological region

P.S. Dineva[a,*], G.D. Manolis[b], T.V. Rangelov[c]

[a] *Department of Continuum Mechanics, Institute of Mechanics, Bulgarian Academy of Sciences, Acad. G. Bonchev Street, B14 Sofia 1113, Bulgaria*
[b] *Department of Civil Engineering, Aristotle University, Thessaloniki GR-54124, Greece*
[c] *Department of Mathematical Physics, Institute of Mathematics and Informatics, Bulgarian Academy of Sciences, 1113 Sofia, Bulgaria*

Received 2 September 2002; accepted 15 April 2003

Abstract

A hybrid boundary integral equation method (BIEM) for transient problems is developed here as a means for investigating ground motion phenomena in geological regions with complex geometry, variable material properties and in the presence of both interface and internal cracks. Two different aspects of the problem are considered, namely computation of (a) ground motions in the form of synthetic seismograms that are manifested at the free surface of the geological region as it is swept by a seismically induced pressure wave and (b) evaluation of the near crack-tip stress concentration field that develops around cracks buried within the deposit for the same type of loading. The present method combines both displacement and regularized traction BIEM in the Laplace transformed domain for the crack-free and cracked states, respectively, while the transient nature of the wave scattering phenomenon is reconstructed through use of the numerical inverse Laplace transformation. Furthermore, plane strain conditions are assumed to hold and the response of the geological region remains within the linear elastic range. The basic strategy, whereby the aforementioned two states are superimposed, has been successfully used in the past for problems in fracture mechanics. Following numerical implementation of the hybrid BIEM, two validation-type examples serve to calibrate the methodology. Finally, the method is used for solving the seismic response of a complex geological region so as to reach a series of conclusions regarding the relative influence of various key parameters of the problem (layering, surface canyon, crack interaction) on the scattered displacement field and on the stress concentration factor.

*Corresponding author.
E-mail addresses: petia@imbm.bas.bg (P.S. Dineva), gdm@civil.auth.gr (G.D. Manolis), rangelov@math.bas.bg (T.V. Rangelov).

0022-460X/$ - see front matter © 2003 Elsevier Ltd. All rights reserved.
doi:10.1016/j.jsv.2003.04.002

1. Introduction

The ability to quantify transient seismic wave fields generated in the vicinity of civil engineering infrastructure is of great importance in any effort to mitigate earthquake effects. Ground motion due to an earthquake is influenced by the dynamic characteristics of the seismic source, the wave propagation path, surface topography, soil layering, plus the mechanical properties of the surrounding geological materials. Therefore, realistic mechanical models for this phenomenon must capture the transient nature of the seismic disturbance, the irregular geometry of the geological region, as well as variations in its material properties. Specifically, site conditions appear mainly in the form of irregular surface topography, non-parallel soft layers (e.g., sedimentary basins) and geological irregularities such as cracks, cavities and inclusions. These local conditions may generate large signal amplifications and motions with spatial variation that must be accounted for in any earthquake-resistant design of dams, bridges, industrial plants, pipeline networks, etc.

Many previous studies have dealt with wave propagation phenomena in geological deposits and the various methods of analysis that have been developed can be briefly classified as follows: (a) analytical solutions for wave motion in alluvial basins of regular shape [1,2]; (b) semi-analytical solutions for wave diffraction by geological irregularities of arbitrary shape [3–5]; (c) approximate techniques such as the ray method, which is based on asymptotic expansions of the wave field [6]. These techniques have been successfully applied to seismological studies at high frequencies [7,8], although it is possible to extend the ray method into the intermediate frequency range [9]; (d) numerical methods are mostly employed in situations where the response is sought within locally inhomogeneous domains, as is the case with soil–structure interaction problems [10–12]. For layered media with irregularities, a variety of numerical techniques have been used. As examples Aki and Larner [13] and Bouchon et al. [14] are mentioned who used the discrete wave number method, Boore [15] who employed finite differences, Nolet et al. [16] who used an approximate modal approach and finally Pedersen et al. [17], Sanchez-Sesma et al. [18], Bouchon et al. [19] and Yokoi and Takenaka [20], who all employed integral equation methods. Also, an indirect-type integral equation method was used by Vai et al. [21] to simulate wave propagation in two-dimensional irregularly layered media with internal line sources. Specifically, results in the form of seismograms were first obtained in the frequency domain followed by Fourier synthesis. Bard and Bouchon [22–24] used the Fourier transform technique for extending the Aki–Larner method [13] to transient analyses of alluvial valleys for both anti-plane and plane strain conditions. Finally, Eshrachi and Dravinski [25,26] examined scattering of elastic waves in two-dimensional multi-layered dipping sediments of arbitrary shape embedded in an elastic half-space by using an integral equation approach; (e) hybrid methods have also appeared in recent years and their basic structure combines finite elements to model interior domains containing all the inhomogeneities, with semi-analytical representations for the exterior regular domain [27]. Among more recent work using hybrid methods in geophysics are those of Furumura et al. [28] and of Panza et al. [29]; (f) The boundary integral equation method (BIEM) has demonstrated many advantages in the solution of elastodynamic problems with infinite or semi-infinite boundaries [30–32]. Specifically, these advantages accrue from a reduction in the dimensions of the problem at hand, implicit satisfaction of the radiation condition associated with unbounded domains, high accuracy in stress concentration computations, flexibility stemming from the semi-analytical

character of the method, and the ability to compute solutions at internal points in terms of boundary values without recourse to full domain discretization. In general, BIEM solutions for engineering problems can be classified as (i) direct analyses in the time-domain [33–35]; (ii) steady state analyses in either Fourier or Laplace transformed domains followed by numerical inversion schemes [36–40]; (iii) the dual boundary element method (DBEM) is primarily used in fracture mechanics, where the displacement-based boundary integral equation (BIE) formulation is used on one side of the crack, while the traction-based BIE is used for the other side [41–43]. A detailed review of the DBEM can be found in Ref. [44]; (iv) dual reciprocity boundary element methods (DRBEM) in either time or transformed domains, where the static fundamental solution is used along with volume discretization schemes [45,46] and finally (v) hybrid approaches that employ finite difference schemes for the time variable and direct BIEM solutions within each time step [47,48]. It should be noted that the term 'hybrid methods' is quite general and implies use of a specific method for a certain part of the problem at hand in conjunction with another method (or a variant of the first) for the remaining part, with the full solution reconstituted through use of superposition.

There seems to be, however, a certain absence of concentrated effort in the development of BIEM codes for efficient computation of ground motions using complex mathematical models for geological deposits with non-parallel interfaces, surface topography and the presence of inclusions and cracks. Also lacking in this field are concurrent computations of stress concentration around discontinuities in the form of near crack-tip fields, which account for interaction phenomena between the discontinuities. The hybrid usage of the displacement-based BIE in continuous layers with interface cracks and of the traction-based, integro-differential BIE in layers with arbitrary placed internal cracks allows for development of a computational package based on the BIEM for solution of transient seismic wave propagation problems through complex geological regions. That, in sum, is the main thrust and contribution of this work. Briefly, the paper is organized as follows: It starts with a definition of the boundary value problem at hand in Section 2, followed by the main part in Section 3 on hybrid usage of both displacement and traction based BIEM for solution of the problem as formulated in the Laplace transform domain. Details concerning numerical solution of the boundary integral equation formulation, as well as synthesis of transient signals are given in Section 4, while test examples that serve to validate the proposed approach are solved in Section 5. Finally, a series of numerical results given in Section 6 for a multi-layered, cracked geological region with surface topography serves as a parametric study from which a number of conclusions can be drawn.

2. Definition of the boundary value problem

A finite, multi-layered cracked geological region $\Omega = \bigcup_{i=1}^{N} \Omega_i$ with non-parallel layers and surface topography is shown in Fig. 1, where the number of layers and cracks is arbitrary. The complement of Ω with respect to the half-space is denoted as Ω_0, while surface topography in region Ω_N is in the form of a semi-circular canyon with radius $r = A$. Soil layers Ω_i, $i = 1, 2, \ldots, N$ are distinguished by virtue of different mechanical properties. Two basic types of cracks are present, namely interface cracks such as FE of length a_{FE} between two soil layers and internal cracks such as MN of length a_{MN} within a soil layer.

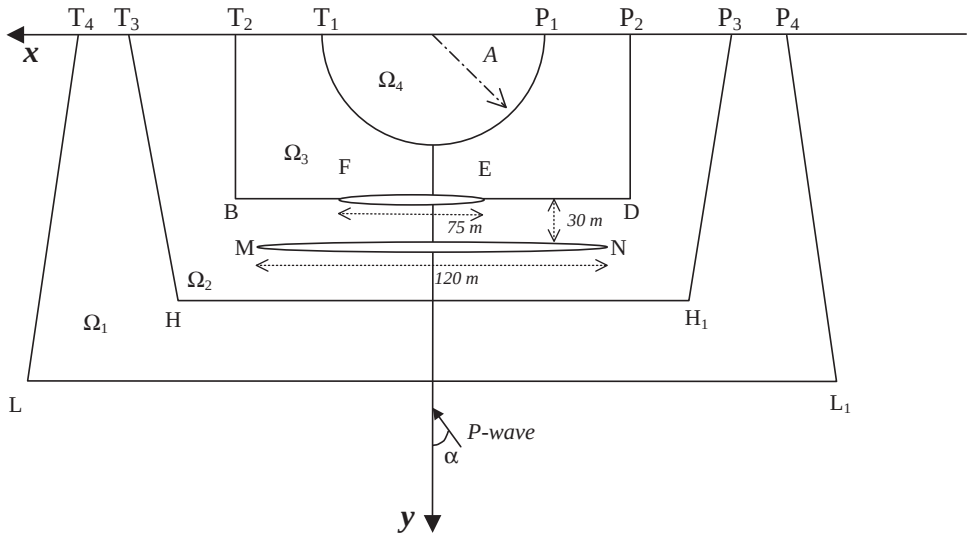

Fig. 1. Layered geological region with surface irregularities and cracks.

A state of plane strain is assumed to hold, and excitation is in the form of a transient longitudinal (or pressure P) wave, which sweeps geological region Ω and produces the following displacement field in Cartesian co-ordinates:

$$(u_x, u_y) = u_0(\sin\alpha\mathbf{i}, -\cos\alpha\mathbf{j}) f(t - (x\sin\alpha - y\cos\alpha)/C_P). \tag{1}$$

In the above, u_x, u_y are the two components of the displacement vector, α is the angle of wave incidence, u_0 is the wave amplitude, t is the time variable and C_P is the P-wave velocity.

Overall, the soil material $\Omega_B = \Omega \cup \Omega_0$, where Ω_0 is the half-space without the geological deposit, is a linear elastic and isotropic solid. Under the usual assumption of small displacements and in the absence of body forces, the governing equations of motion are

$$(C_P^2 - C_S^2)u_{j,ji}(x,y,t) + C_S^2 u_{i,jj}(x,y,t) = \ddot{u}_i(x,y,t) \tag{2}$$

in $Q_B = \Omega_B \times (0,T)$, where indices i, j range as (1,2), while commas and dots, respectively, indicate space and time derivatives. Furthermore, $C_P^2 = (\lambda + 2\mu)/\rho$; $C_S^2 = \mu/\rho$ are longitudinal and shear (S) wave velocities that differ for each layer Ω_i, λ and μ are Lame's constants, ρ is the mass density, and T is the total duration of the dynamic phenomenon.

Tractions were prescribed on the S_p part of the boundary and displacements on the complementary part S_u, where $S_B = S_p \cup S_u$, $S_p \cap S_u = \varnothing$. More specifically, the boundary conditions are as follows:

(a) All tractions are zero on the free surface, i.e., $p_i(x,0,t) = 0$.
(b) The influence of the geological deposits on the motion in the underlying half-space vanishes at sufficiently large distances, i.e., Sommerfeld's radiation condition holds.
(c) Continuity and dynamic equilibrium are both satisfied at the boundary between any two soil layers, namely $u_i(x,y,t)|_{S_{\Omega_i}} = u_i(x,y,t)|_{S_{\Omega_{i+1}}}$ and $p_i(x,y,t)|_{S_{\Omega_i}} = -p_i(x,y,t)|_{S_{\Omega_{i+1}}}$.

(d) At the common interface between deposits and half-space, the boundary condition $u_i(x,y,t)|_{T_4LL_1P_4} = u_i^{fr}(x,y,t)|_{T_4LL_1P_4}$ is satisfied for any $(x,y) \in T_4LL_1P_4$, with superscript fr denoting free-field motion. This free motion in turn consists of the wave field from the incident P-wave traveling in half-space Ω_0 with constant material properties. It is simple to show [49] that the transient response $u_i^{fr}(x,y,t)$ in the half-space from the P-wave of Eq. (1) is given as $u_i^{fr}(x,y,t) = 1/2\pi i \int_{b-i\infty}^{b+i\infty} U_i^{fr}(x,y,s)e^{st}\,ds$. Here one has $U_i^{fr}(x,y,s) = u_{0i}\,\bar{h}(x,y,s)\,\bar{f}(s)$ which is the free-field motion in the Laplace transformed domain and u_{0i} is a unit vector which represents direction of motion. Also, $\bar{h}(x,y,s)$ is the equivalent of the unit impulse motion in the Laplace transform domain resulting from an incident P-wave of unit strength, i.e., $\delta(t-(x\sin\alpha - y\cos\alpha)/C_P)$, and $\bar{f}(s)$ is the Laplace transform of $f(\tau)$. This approach implies that a state of uniform ground motion is induced by the incoming P-waves. This, of course, may no longer be true if the overall dimensions of the geological region are large compared to some epicentre distance, in which case spatially variable ground motions are observed [50]. In that case, free-field motions become quite complex and their Laplace transform has to be evaluated by numerical means.

(e) On a crack boundary $S_{cr} = S_{cr}^+ \cup S_{cr}^-$, the tractions are given as

$$p_i(x,y,t)|_{S_{cr}^-} = -p_i(x,y,t)|_{S_{cr}^+}, \tag{3}$$

where S_{cr}^+, S_{cr}^-, respectively, are upper and lower crack surfaces.

Finally, initial conditions at $t = 0$ in Ω_B are as follows:

$$u_i(x,y,0) = u_{0i}(x,y), \quad \dot{u}_i(x,y,0) = \dot{u}_{0i}(x,y). \tag{4}$$

In sum, any solution to the above boundary value problem is a vector-value function $u_i(x,y,t) \in C^2(Q_B) \cap C^1(\bar{Q}_B)$, from which tractions $p_i(x,y,t) \in C^1(Q_B) \cap C(\bar{Q}_B)$ derive, and which satisfies Eq. (2), boundary conditions (a)–(e) and the initial conditions. Note that $C^k(R)$ denotes the set of k-times continuously differentiable functions in space R.

3. Hybrid BIEM formulation in the Laplace domain

The Laplace transform is used here in order to suppress the independent time variable and to account for any initial conditions. Application of the aforementioned transformation to the governing equations of motion (2) yields a system of elliptic partial differential equations, amenable to numerical solution by the combined displacement-based BIE for layers without cracks (or interface cracks only) and hypersingular, traction-based BIE for layers with internal cracks. It can be noted in passing that this type of approach, where the crack-free and cracked states are superimposed, has been used in fracture mechanics and a similar type of BIEM formulation was recently developed in the frequency domain by Dineva and Manolis [51,52], which was shown to be an efficient numerical tool for time-harmonic wave-scattering problems in geological regions.

Using the Laplace transform, where $\bar{f}(s) = \int_0^\infty f(t)\exp(-st)\,dt$ is the direct transformation (provided $f(t)$ is locally integrable along interval $[0, \infty)$) and

$$f(t) = \frac{1}{2\pi i}\int_{b-i\infty}^{b+i\infty} \bar{f}(s)\exp(st)\,ds$$

is the inverse transformation (with b greater than the real part of all singularities of $\bar{f}(s)$), the combined equations of motion (2) and initial conditions (4) assume the following form:

$$(C_P^2 - C_S^2)\bar{u}_{k,ki} + C_S^2\bar{u}_{i,kk} = s^2\bar{u}_i - \frac{1}{\rho}\bar{F}_i. \tag{5}$$

Also, the forcing function term is now

$$\bar{F}_i(x, y, s) = \rho[su_{0i}(x, y) + \dot{u}_{0i}(x, y)]. \tag{6}$$

Eq. (5) have to be solved in conjunction with the transformed boundary conditions for a finite set of discrete values of the Laplace parameter s. Once a sufficiently large spectrum of values is obtained for the solution, numerical inversion is performed on selective dependent variables to obtain the desired transient response.

3.1. The BIEM formulation

For a linear boundary value problem, superposition holds and the total displacement $\bar{u}_i$ and traction $\bar{p}_i$ fields in the Laplace transformed domain are written in the form

$$\{\bar{u}_i, \bar{p}_i\} = \{\bar{u}_i^0, \bar{p}_i^0\} + \{\bar{u}_i^c, \bar{p}_i^c\}, \tag{7}$$

where $\bar{u}_i^0(\mathbf{r}, s), \bar{p}_i^0(\mathbf{r}, s)$ comprise the continuous transient field in the crack-free body. Next, $\bar{u}_i^c(\mathbf{r}, s), \bar{p}_i^c(\mathbf{r}, s)$ are due to the presence of cracks [53] and are produced by loads $\bar{p}_i^c(\boldsymbol{\eta}, s) = -\bar{p}_i^0(\boldsymbol{\eta}, s)$ acting across local co-ordinate $\boldsymbol{\eta} \in S_{cr} = S_{cr}^+ \cup S_{cr}^-, S_{cr} = EF \cup MN$, while all other loads are zero on S_p, on S_u and on the external boundary $T_4LL_1P_4$. Wave field $\bar{u}_i^0(\mathbf{r}, s), \bar{p}_i^0(\mathbf{r}, s)$ is in turn a superposition of free-field motions $\{\bar{u}_i^{fr}, \bar{p}_i^{fr}\}$ and scattered waves $\{\bar{u}_i^{sc}, \bar{p}_i^{sc}\}$ in the layered geological deposit, i.e.,

$$\{\bar{u}_i^0, \bar{p}_i^0\} = \{\bar{u}_i^{fr}, \bar{p}_i^{fr}\} + \{\bar{u}_i^{sc}, \bar{p}_i^{sc}\}. \tag{8}$$

As far as boundary conditions for the crack-free body are concerned, it is found that

(a) The surface of the half-space is traction-free, i.e., $\bar{p}_i^0(x, 0, s) = 0$.
(b) The Sommerfield radiation condition is satisfied at infinity.
(c) Across any two consecutive layers, both continuity and equilibrium are satisfied as

$$\bar{u}_i^{sc}|_{S_{\Omega_i}} = \bar{u}_i^{sc}|_{S_{\Omega_i+1}} \quad \text{and} \quad \bar{p}_i^{sc}|_{S_{\Omega_i}} = -\bar{p}_i^{sc}|_{S_{\Omega_i+1}}.$$

(d) Continuity is also satisfied at the boundary between geological deposit and underlying half-space $T_4LL_1P_4$ as $\bar{u}_i^{sc}(x, y, s)|_{T_4LL_1P_4} = \bar{u}_i^{fr}(x, y, s)|_{T_4LL_1P_4}$.

The boundary conditions for the cracked geological continuum are as follows:

(a) On the surface of the half-space, $\bar{p}_i^c(x, 0, s) = 0$.
(b) Tractions $\bar{p}_i^c(\boldsymbol{\eta}, s) = -\bar{p}_i^0(\boldsymbol{\eta}, s)$ for $\boldsymbol{\eta} \in S_{cr}, S_{cr} = EF \cup MN$.
(c) Sommerfeld's radiation is again satisfied at infinity.
(d) As before, continuity and dynamic equilibrium across a layer interface dictates that $\bar{u}_i^c|_{S_{\Omega_i}} = \bar{u}_i^c|_{S_{\Omega_i+1}}$ and $\bar{p}_i^c|_{S_{\Omega_i}} = -\bar{p}_i^c|_{S_{\Omega_i+1}}$.
(e) Along the interface between the geological deposit and half-space $T_4LL_1P_4$, boundary condition $\bar{u}_i^c|_{T_4LL_1P_4} = 0$ is satisfied.

In order to solve the above problem, it is necessary to formulate a set of displacement and traction-based BIEs, beginning with the 'crack-free' state, for which the conventional, displacement BIEM is employed separately in each layer as

$$C_{ij}\bar{u}_j^0(\mathbf{r},s)=\int_{\Gamma_{\Omega_m}} U_{ij}^*(\mathbf{r},\mathbf{r}_0,s)\bar{p}_j^0(\mathbf{r}_0,s)\,\mathrm{d}\Gamma-\int_{\Gamma_{\Omega_m}} P_{ij}^*(\mathbf{r},\mathbf{r}_0,s)\bar{u}_j^0(\mathbf{r}_0,s)\,\mathrm{d}\Gamma \tag{9}$$

In the above, $m=1,2,3,\ldots,N$; total surface $S_B=\Gamma_{\Omega_1}\cup\Gamma_{\Omega_2}\cdots\cup\Gamma_{\Omega_i}\cdots\cup\Gamma_{\Omega_N}\cup S_{cr}$; C_{ij} are jump terms dependent on the local geometry at collocation node $\mathbf{r}$; nodes $\mathbf{r},\mathbf{r}_0$ denote the position vectors of the receiver (field) and source (integration) points, respectively; U_{ij}^*,P_{ij}^* are the singular displacement and traction fundamental solutions (kernel functions) of Eq. (5) originally derived in Refs. [36,37]; and finally, Γ_{Ω_m} is the boundary of the Ω_m layer.

In the cracked state, vector field $\{\bar{u}_i^c,\bar{p}_i^c\}$ satisfies two types of BIEs. Specifically,

(a) For any layer Ω_m without internal cracks, the following displacement BIE is used:

$$C_{ij}\bar{u}_j^c(\mathbf{r},s)=\int_{\Gamma_{\Omega_m}} U_{ij}^*(\mathbf{r},\mathbf{r}_0,s)\bar{p}_j^c(\mathbf{r}_0,s)\,\mathrm{d}\Gamma-\int_{\Gamma_{\Omega_m}} P_{ij}^*(\mathbf{r},\mathbf{r}_0,s)\bar{u}_j^c(\mathbf{r}_0,s)\,\mathrm{d}\Gamma. \tag{10}$$

(b) For any layer Ω_n with an internal crack, the displacement BIE formulation degenerates and it becomes necessary to introduce a hyper-singular traction BIE. Regularization of this formulation [54] yields the following system of equations:

$$\begin{aligned}\bar{p}_l^c(\boldsymbol{\xi}^+,s)=&-\bar{p}_l^0(\boldsymbol{\xi}^+,s)=\int_{\Gamma_{\Omega_n}} P'_{lk}U_{ks}^*(\boldsymbol{\eta},\boldsymbol{\xi}^+,s)\bar{p}_s^c(\boldsymbol{\eta},s)\,\mathrm{d}S_\eta\\&+c_{lpjr}n_p(\boldsymbol{\xi}^+)\left\{c_{iskt}\left[\int_{S_{cr}^+}\Delta K_{rs}^i D_t U_{kj}^*(\boldsymbol{\eta}-\boldsymbol{\xi}^+,s)\,\mathrm{d}S_\eta+\int_{\Gamma_{\Omega_n}} K_{rs}^i D_t U_{kj}^*(\boldsymbol{\eta}-\boldsymbol{\xi}^+,s)\,\mathrm{d}S_\eta\right]\right.\\&\left.+\rho s^2\left[\int_{S_{cr}^+}\Delta\bar{u}_i^c(\boldsymbol{\eta},s)n_r(\boldsymbol{\eta})U_{ij}^*(\boldsymbol{\eta}-\boldsymbol{\xi}^+,s)\,\mathrm{d}S_\eta+\int_{\Gamma_{\Omega_n}}\bar{u}_i^c n_r(\boldsymbol{\eta})U_{ij}^*(\boldsymbol{\eta}-\boldsymbol{\xi}^+,s)\,\mathrm{d}S_\eta\right]\right\},\end{aligned} \tag{11}$$

$$\begin{aligned}\bar{p}_l^c(\boldsymbol{\xi}^*,s)=&\int_{\Gamma_{\Omega_n}} P'_{lk}U_{ks}^*(\boldsymbol{\eta},\boldsymbol{\xi}^*,s)\bar{p}_s^c(\boldsymbol{\eta},s)\,\mathrm{d}S_\eta\\&+c_{lpjr}n_p(\boldsymbol{\xi}^*)\left\{c_{iskt}\left[\int_{S_{cr}^+}\Delta K_{rs}^i D_t U_{kj}^*(\boldsymbol{\eta}-\boldsymbol{\xi}^*,s)\,\mathrm{d}S_\eta+\int_{\Gamma_{\Omega_n}} K_{rs}^i D_t U_{kj}^*(\boldsymbol{\eta}-\boldsymbol{\xi}^*,s)\,\mathrm{d}S_\eta\right]\right.\\&\left.+\rho s^2\left[\int_{S_{cr}^+}\Delta\bar{u}_i^c(\boldsymbol{\eta},s)n_r(\boldsymbol{\eta})U_{ij}^*(\boldsymbol{\eta}-\boldsymbol{\xi}^*,s)\,\mathrm{d}S_\eta+\int_{\Gamma_{\Omega_n}}\bar{u}_i^c n_r(\boldsymbol{\eta})U_{ij}^*(\boldsymbol{\eta}-\boldsymbol{\xi}^*,s)\,\mathrm{d}S_\eta\right]\right\}.\end{aligned} \tag{12}$$

In terms of notation, tensor $c_{ijkl}=\lambda\delta_{ij}\delta_{kl}+\mu(\delta_{ik}\delta_{jl}+\delta_{il}\delta_{kj})$, P' is the stress operator, tractions $\bar{p}_l^0(\boldsymbol{\xi}^+,s)$ are obtained from the crack-free state solutions, tangential derivatives $K_{rs}^i=[n_r(\boldsymbol{\eta})D_s-n_s(\boldsymbol{\eta})D_r]\bar{u}_i(\boldsymbol{\eta},p)$ and $\Delta K_{rs}^i=[n_r(\boldsymbol{\eta})D_s-n_s(\boldsymbol{\eta})D_r]\Delta u_i(\boldsymbol{\eta},s)$, $D_r=\partial/\partial\eta_r$ are partial derivatives, $\boldsymbol{\xi}^+$, $\boldsymbol{\xi}^*$ are field points on S_{cr}^+ and Γ_{Ω_n}, respectively, and finally $\Delta u_i^c=u_i^{c+}-u_i^{c-}$ is the crack-opening displacement (COD) representing a displacement discontinuity across the crack surfaces. When a surface crack intersects the outer boundary, all equations

written above for an internal crack in a finite elastic body are still valid, provided that $\boldsymbol{\xi}^{+} \in S_{cr}^{+} \backslash (S_{cr}^{+} \cap S_B)$, $\boldsymbol{\xi}^{*} \in S_B \backslash (S_B \cap S_{cr}^{+})$.

The primary unknowns of this type of boundary value problem are displacement and traction fields $\bar{u}_i^0(\mathbf{r}, s), \bar{p}_i^0(\mathbf{r}, s)$ and $\bar{u}_i^c(\mathbf{r}, s), \bar{p}_i^c(\mathbf{r}, s)$ on S_B, plus crack opening displacements $\Delta\bar{u}_i^c(\boldsymbol{\eta}, s)$ on S_{cr}^{+}. Inasmuch as Eqs. (11) and (12) are boundary integro-differential equations (BIDE), functions $K_{rs}^i \bar{u}_i(\boldsymbol{\eta}, s)$ and $\Delta K_{rs}^i \Delta\bar{u}_i(\boldsymbol{\eta}, s)$ corresponding to tangential derivatives of the displacements must be considered as unknowns.

4. Numerical solution procedure

In this section, some aspects of the numerical solution procedure, particular to the present BIEM implementation, are discussed. More specifically, the following points were focussed on:

(a) In a mixed-mode crack problem, where both crack tips are modelled by a single domain, the BIEM solution degenerates [39,40]. This can be avoided by introducing a hybrid usage of the displacement-based BIE formulation for layers with interface cracks only, and of the traction-based BIE formulation for layers containing internal cracks.

(b) Careful modelling of the crack-tip singularity is required in order to capture the correct asymptotic behaviour of displacement and traction fields near the edges of a crack. In the present implementation, crack-tip singularities are modelled by the quarter-point boundary element (QP-BE), which reproduces the $\sqrt{r}$ asymptotic behaviour of the displacement field, and by the singular traction quarter-point boundary element (SQP-BE), which follows the $1/\sqrt{r}$ asymptotic behaviour of traction field [53] as shown in Fig. 2a.

(c) The traction-based BIE is hypersingular due to the presence of derivatives of the traction fundamental solution and some of the resulting integrals do not converge, even in the Cauchy principle-value (CPV) sense. To circumvent this difficulty, a regularization procedure is used here based on integration by parts, so as to shift the spatial derivatives from the traction fundamental solution to the unknown displacements in the BIE statement [54].

(d) A polynomial approximation of the boundary geometry, as well as of the displacement and traction vectors, which employs continuous shape functions (at least across the collocation points) is used. For the regularized traction-based BIE, additional smoothness requirements are necessary for the displacement field due to the presence of tangential derivatives. The regular BE are of the parabolic type, so that discretization satisfies Hölder continuity for the displacements and tractions at internal nodes only. At edge nodes, the source points are shifted [55,56], but the element nodes remain at the edges in order to satisfy Hölder continuity for the tractions and the tangential displacement derivatives.

(e) Careful numerical treatment is necessary for edges and corners in the boundary element mesh used for the finite geological region. For the displacement-based BIE, only continuity of the displacement components at the nodes is required; naturally, corners can be used as collocation points. For the traction-based BIE, additional continuity of the derivatives of the displacements at an element node is required; thus, corner nodes can no longer be used as collocation points and must be shifted inwards [55,56].

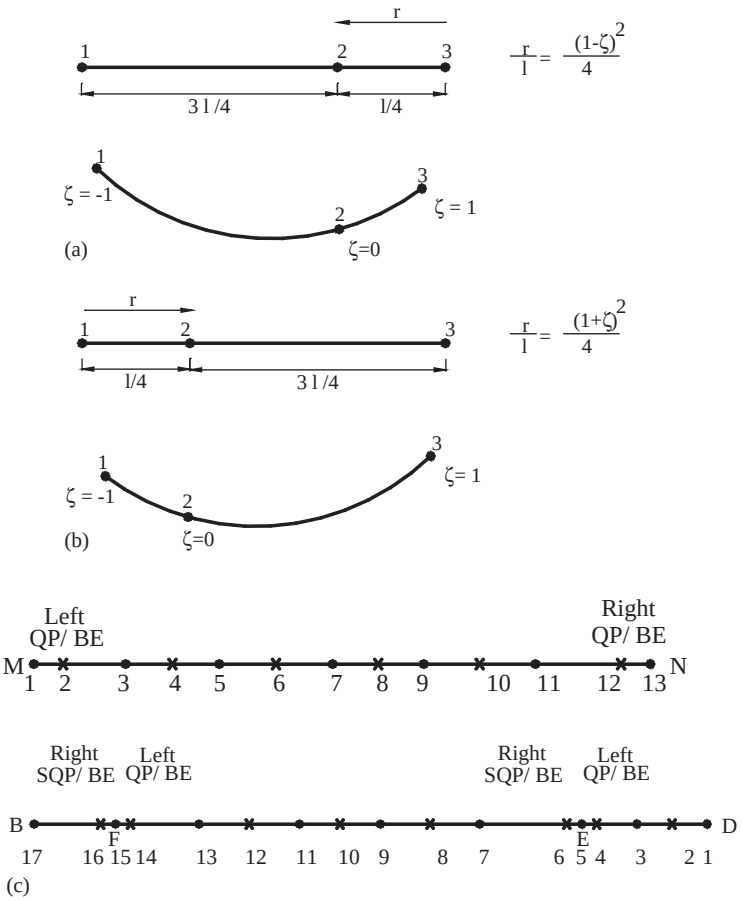

Fig. 2. (a) Crack-tip QP-BE and (b), (c) crack discretization schemes respectively involving the *MN* internal crack and the *EF* interface crack along boundary *B–D*.

(f) Overall accuracy of the BIEM is highly dependent on the precision by which the various regular and singular integrals appearing in the formulation are evaluated. Standard 32-point Gaussian quadrature is used for computing all regular integrals. The singular integrals are evaluated analytically, based on asymptotic expansions of the fundamental solutions for small arguments. The singular integrals are of the general type $\int_{-1}^{1} \frac{Q_l(\xi)}{(\xi-a)} \mathrm{d}\xi$, $\xi \in [-1,+1]$, with $Q_l(\xi)$ a polynomial of degree l. These integrals can always be written as the sum of regular plus CPV-type integrals. It is possible to apply asymptotic expansions for the kernels, either along the entire BE length or in a small region of exclusion around the collocation point. In the latter case, numerical integration by Gaussian quadrature can be used beyond this small region. The extent of the neighbourhood of exclusion around a collocation point depends on the values of the Bessel function arguments that appear in the kernel functions, which in turn are controlled by the minimum/maximum BE length and by the incident wavelength.

As far as stress intensity factor (SIF) calculation accuracy is concerned, consider for example the node numbering of the crack-tip QP BE as (1), (2) and (3), where node (3) is the crack-tip and

$\Delta u_i^{(3)} = 0$, as shown in Fig. 2b. Furthermore, the length of QP-BE is denoted by l_{cr}^d, the length of the near crack-tip SQP- BE by l_{cr}^t and the value of the traction at the second node of the SQP-BE by $\bar{p}_i^{tr}$, i.e., point $(a + l_{cr}^t/4)$. Next, the two-point displacement SIF formula and the traction SIF formula for an internal crack [57] are

$$\begin{cases} K_{\mathrm{I}}^{d1} = \dfrac{2}{(\kappa+1)k_s^2\sqrt{\pi a}}\sqrt{\dfrac{2\pi}{l_{cr}^d}}\,\Delta u_2^{(2)}, \\ K_{\mathrm{II}}^{d1} = \dfrac{2}{(\kappa+1)k_s^2\sqrt{\pi a}}\sqrt{\dfrac{2\pi}{l_{cr}^d}}\,\Delta u_1^{(2)}, \end{cases} \tag{13}$$

$$\begin{cases} \bar{K}_{\mathrm{I}}^{d2} = \dfrac{1}{(\kappa+1)k_s^2\sqrt{\pi a}}\sqrt{\dfrac{2\pi}{l_{cr}^d}}\,(4\Delta\bar{u}_2^{(2)} - \Delta\bar{u}_2^{(1)}), \\ \bar{K}_{\mathrm{II}}^{d2} = \dfrac{1}{(\kappa+1)k_s^2\sqrt{\pi a}}\sqrt{\dfrac{2\pi}{l_{cr}^d}}\,(4\Delta\bar{u}_1^{(2)} - \Delta\bar{u}_1^{(1)}) \end{cases} \tag{14}$$

and

$$\begin{cases} \bar{K}_{\mathrm{I}}^{t} = \dfrac{1}{\mu k_s^2\sqrt{\pi a}}\sqrt{\dfrac{\pi l_{cr}^t}{2}}\,\bar{p}_1^{tr}, \\ \bar{K}_{\mathrm{II}}^{t} = \dfrac{1}{\mu k_s^2\sqrt{\pi a}}\sqrt{\dfrac{\pi l_{cr}^t}{2}}\,\bar{p}_2^{tr}, \end{cases} \tag{15}$$

respectively, where parameter $k = 3 - 4\nu$ (ν is the Poisson ratio). The overall SIF at the crack tips of an interface crack is calculated [58] as

$$\bar{K}_0 = \frac{1}{D_\varepsilon\sqrt{(1+4\varepsilon^2)}\sqrt{l_{QP-BE}}}\sqrt{(4\Delta\bar{u}_2^{(2)} - \Delta\bar{u}_2^{(1)})^2 + (4\Delta\bar{u}_1^{(2)} - \Delta\bar{u}_1^{(1)})^2}, \tag{16}$$

where ε is the well-known bimaterial constant, while both D_ε and ε depend on the material constants of the layers at both sides of the interface.

Finally, in reference to the inverse Laplace transformation, the boundary value problem is solved as described in Section 2 in numerical form and as a function of Laplace parameter s. Next, the inversion algorithm described in Ref. [59] is used. Specifically, let $[0, T]$ be the total time interval of interest and $t_j = jT/N,\ j = 0, \ldots, N-1$ the time step, where L, N are positive integers. In order to recover the original time dependence, function $f(t)$ is calculated at a set of discrete points t_j from the transformed spectrum $\bar{f}(s_n)$ by the following quadrature formula:

$$f(t_j) = \frac{2}{T}\mathrm{e}^{bt_j}\left[-\frac{1}{2}\,\mathrm{Re}(\bar{f}(b)) + \mathrm{Re}\left(\sum_{j=0}^{N-1}(A_n + \mathrm{i}B_n)W^{jn}\right)\right], \tag{17}$$

where

$$A_n = \sum_{l=0}^{L}\mathrm{Re}\,\bar{f}\left(b + \mathrm{i}(n+lN)\frac{2\pi}{T}\right), \quad B_n = \sum_{l=0}^{L}\mathrm{Im}\,\bar{f}\left(b + \mathrm{i}(n+lN)\frac{2\pi}{T}\right). \tag{18}$$

Also, $l = 0, \ldots, L$, $n = 0, \ldots, N$ and $W = \exp(i2\pi/N)$ is a complex root of unity. For a spectrum of values equal to $LN \in [50, 5000]$, an optimum choice is $bT \in [5, 10]$ in order to have accurate results. Thus, the time-dependent displacements $u_i(x, y, t)$ and tractions $p_i(x, y, t)$ of the boundary value problem at hand are recovered for $t \in [0, T]$, starting with a spectrum of values dictated by the discrete form of the Laplace transform parameter $s_n = b + in(2\pi)/T$, $n = 0, \ldots, N$. It is noted at this point that fast Fourier transform (FFT) concepts [59,60] are used in calculating coefficients A_n, B_n of Eq. (18). It is also possible to compute the direct Laplace transform $\bar{f}(s)$ of an arbitrary function of time $f(t)$, for which an analytical expression cannot be found, by modifying the above algorithm. This type of exercise does not appear in the literature, but was carried out within the framework of the present research effort [61].

5. Validation study

In this section, two test cases are solved using the hybrid BIEM developed above so as to gauge its accuracy and efficiency for transient problems involving cracks in continuous media.

5.1. Diffraction of elastic waves by a finite crack in the infinite plane

The first case solves a crack of length $(-a, +a)$ along the horizontal axis Ox impinged upon by an incident plane wave, whose normal is at an angle θ with respect to the horizontal, as shown in Fig. 3. The crack itself is assumed traction-free. The governing equation of motion for this problem is Eq. (5) in the Laplace transform domain under zero initial conditions and in the absence of any body forces. Inasmuch as the BIEM developed herein is based on the combined usage of displacement and traction-based BIE, a first test example for P-waves was solved by the traction BIE, while a second test example for SV-waves was solved by the displacement BIE. For brevity, only the former results are shown here; the latter ones can be found in the relevant research report [61].

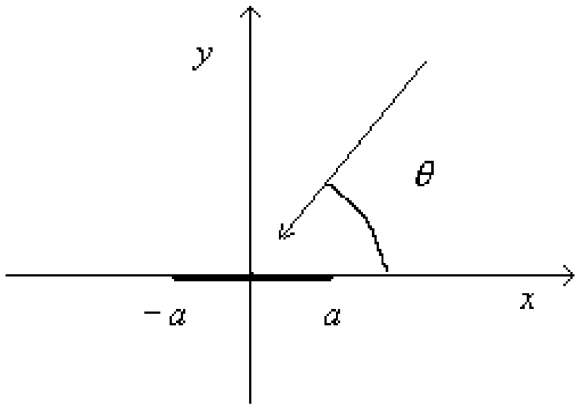

Fig. 3. Incident wave in the cracked plane.

The transient incident wave in the Laplace domain is defined by the following potentials:

$$\bar{u}_1 = \partial_1 \bar{\Phi} + \partial_2 \bar{\Psi}, \quad \bar{u}_2 = \partial_2 \bar{\Phi} - \partial_1 \bar{\Psi}. \tag{19}$$

In the above,

$$\begin{cases} \Phi = f\left(\alpha t - \dfrac{\alpha}{C_P}(x\cos\theta + y\sin\theta)\right), \\ \Psi = g\left(\beta t - \dfrac{\beta}{C_S}(x\cos\theta + y\sin\theta)\right) \end{cases} \tag{20}$$

while α, β are constants and functions Φ, Ψ satisfy Eq. (2) provided $f, g \in C^2(R)$. For P-waves, functions $f(\tau) = 0.5(\mathrm{H}(\tau)\tau)^2, g = 0$ where $\mathrm{H}(\tau)$ is the Heaviside step function.

Numerical solution of integro-differential equations (11) and (12) in the Laplace transform domain was programmed using a Fortran 90 compiler. Input data for a crack in a continuous medium consists of (i) material constants λ, μ, ρ, v; (ii) length and position of the line crack along the Ox axis and (iii) Laplace transform data of the incident traction $\bar{p}_i^{in}$ on S_{cr}. Output is in the form of COD $\Delta\bar{u}_i$ on S_{cr}. Following the numerical inverse Laplace transformation quantified by Eqs. (17) and (18), a displacement solution is finally reconstructed in the time domain.

More specifically, the crack examined herein has length $2a = 10$ m and is buried in an elastic geological continuum whose material constants have the following numerical values: $\lambda = \mu = 2.2 \times 10^{10}$ Pa, $v = 0.25$ and $\rho = 2400$ kg/m^3. The number of BE for modelling the crack are five. More specifically, the first element is a left QP-BE, the second through fourth elements are ordinary BE, and the fifth one is a right QP-BE. Their corresponding lengths respectively are $l_1 = 0.75,\ l_2 = 2.8,\ l_3 = 2.9,\ l_4 = 2.8,\ l_5 = 0.75$; furthermore, it is found that $l_{cr}^d = 0.75, l_{cr}^t = 1$. The numerical inversion algorithm employs $N = 250$ spectrum points and the real part of the Laplace transform parameter s is set as equal to $b = 6.0/T$.

Fig. 4 plots the SIF obtained for an angle of P-wave incidence of $\theta = \pi/2$ and normalized by factor $\rho\sqrt{\pi a}$, along with the results of Chirino and Dominguez [40], who used the displacement BIE in the Fourier domain. The comparison is good and shows that the numerical solution achieved by the traction-based BIE is accurate.

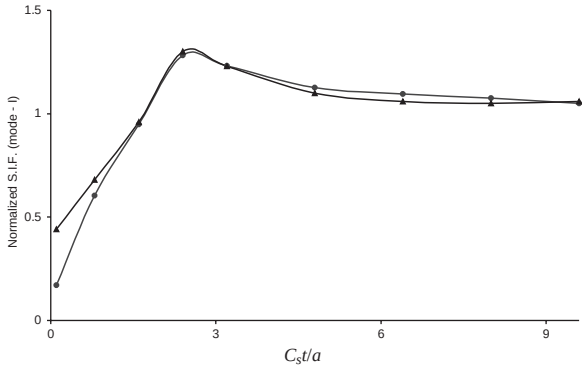

Fig. 4. Comparison study for Mode I SIF: -●-, present results; -▲-, Chirino and Dominguez results.

5.2. Transient response of a cracked rectangular plate under uniform traction

The geometry of the problem is given in Fig. 5, along with modelling details. This example was first solved by Chen [62] who used finite differences, while a subsequent solution by Murti and Valliappan [63] employed the finite element method. Solutions to this benchmark problem were also obtained by Jiaju and Xing [64] using the BIEM coupled with the inverse Laplace transformation algorithm of Durbin [59] and by Chirino and Dominguez [40], who used a BIEM defined in the frequency domain with the fast Fourier transformation for recovering the transient mode I SIF.

The size of the plate is 20×40 mm, while its material constants have the following values: shear modulus $\mu = 7.7 \times 10^{10}$ Pa, density $\rho = 5000$ kg/m^3 and the Poisson ratio $v = 0.3$. There is a crack of length $2a = 5$ mm in the middle of the plate, while the externally imposed load is a suddenly applied and maintained traction $\sigma H(t)$, where $\sigma = 400 \times 10^6$ Pa. Due to symmetry, only one-quarter of the plate need be analysed. As far as modelling the crack is concerned, a QP-BE and a traction SQP-BE are used on both sides of the crack tip with $l_{QP-BE} = l_{SQP-BE} = 0.5$ mm. The duration of the loading event is $T = 0.012$ ms, and the parameters used in conjunction with the Laplace inversion algorithm are the same as before, namely $b = 6.0/T$ and $N = 250$.

A comparison of the results obtained by the present method with those of Jiaju and Xing [64] is given in Fig. 6a, where the magnitude of SIF has been normalized by $\sigma\sqrt{\pi a}$. Further comparisons with the other solutions appear in Fig. 6b. In all cases, agreement between the various results is very good. Chirino and Dominguez [40] have concluded that their FFT results for the purely elastic plate material show spurious oscillations that can be traced to numerical inaccuracies. FFT

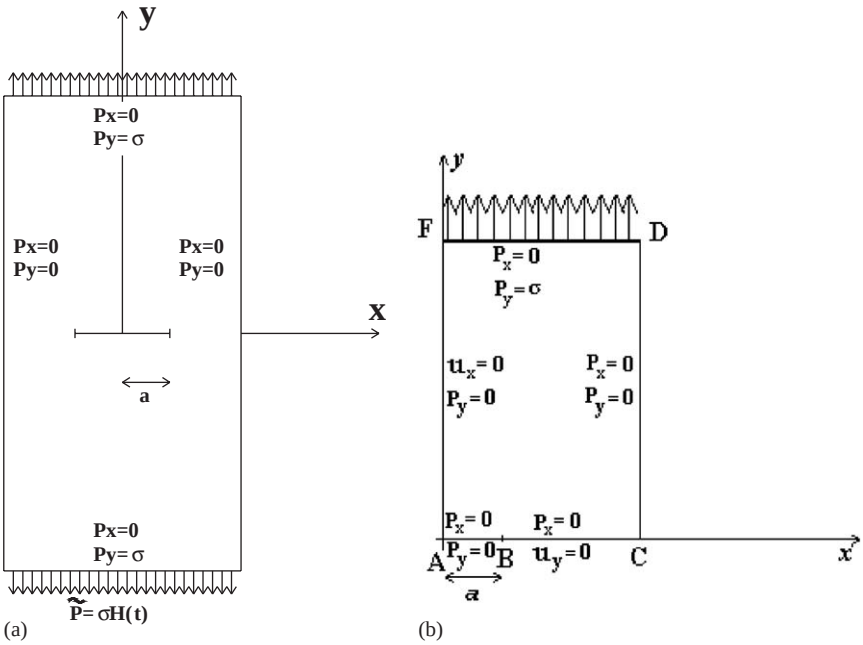

Fig. 5. (a) Cracked plate and (b) quarter model for the plate with $l_{SQP} = 0.5$ mm.

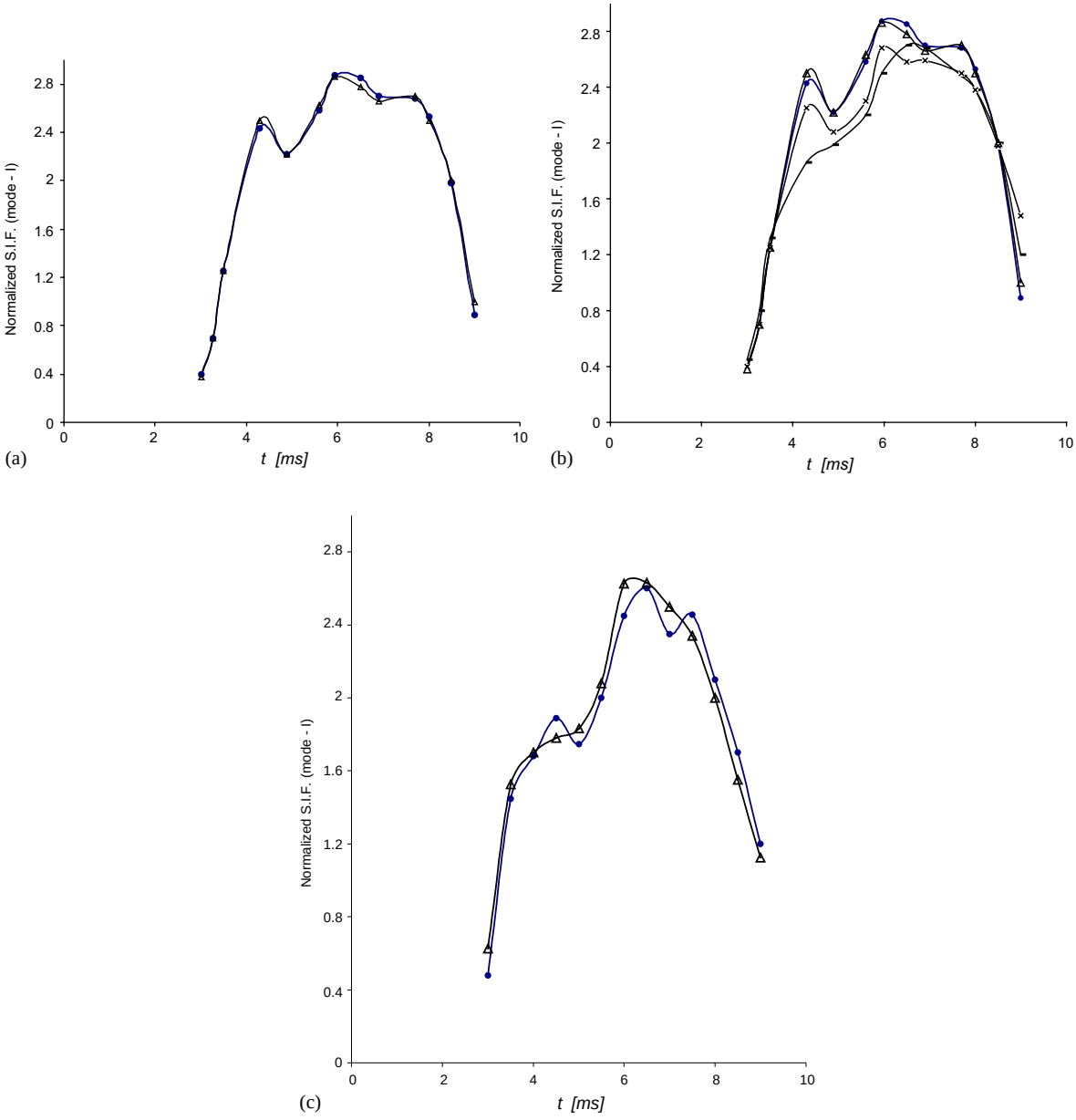

Fig. 6. Transient mode I SIF normalized by $\sigma H(t)\sqrt{\pi a}$ for cracked plate under uniform step traction. (a, b) elastic material: -●-, present results, -△-, Jiaju and Xing results; –, Chen's results; -×-, Murti's results. (c) Material with 1% internal damping: -●-, present results; -△-, Dominguez and Chirino results.

filtering ameliorates this problem, but so does the presence of some internal (material) damping. In this study, it was quite simple to introduce a small amount of internal damping in the plate through the use of complex material moduli in the form $\mu_c = \mu(1 + 2i\beta)$, with a dimensionless damping coefficient β in the range 1–5%. Fig. 6c shows the comparison between our results and

Table 1
Properties of the geological deposit

Soil layer	Upper boundary	Crack boundary	Lower boundary	Lateral boundary at free surface
(a) *Geometry*				
3	Semi-circle radius $A = 30$ m	Interface crack FE F: $(45, 90)$ E: $(-30, 90)$	Broken line T_2BFEDP_2 T_2: $(60, 0)$; T_1: $(30, 0)$ B: $(60, 90)$; D: $(-60, 90)$ P_2: $(-60, 0)$; $P_1(-30, 0)$	$T_2T_1 \cup P_1P_2$
2	Broken line T_2BFEDP_2	Interface crack FE and internal crack MN Configuration 1: M: $(60, 120)$; N: $(-60, 120)$ Configuration 2: M: $(-33, 120)$; N: $(-75, 120)$ Configuration 3: M: $(60, 170)$; N: $(-60, 170)$	Broken line $T_3HH_1P_3$ T_3: $(90, 0)$; H: $(75, 180)$ H_1: $(-75, 180)$; P_3: $(-90, 0)$	$T_3T_2 \cup P_2P_3$
1	Broken line $T_3HH_1P_3$		Broken line $T_4LL_1P_4$ T_4: $(100, 0)$; L: $(110, 270)$ L_1: $(-110, 270)$; P_4: $(-100, 0)$	$T_4T_3 \cup P_3P_4$

Soil layer	Type of soil	Material density ρ (kg/m^3)	Lame constant λ (Pa)	Shear modulus μ (Pa)	The Poisson ratio v	S-wave velocity C_S (m/s)	P-wave velocity C_P (m/s)
(b) *Material properties*							
3	Lime-stone I	2400	19.6×10^9	20.2×10^9	0.25	2900	5000
2	Lime-stone II	2800	23.6×10^9	16.5×10^9	0.29	2430	4500
1	Granite I	2800	35.3×10^9	24.7×10^9	0.29	2970	5500
Half-space	Granite II	3000	25.4×10^9	24.5×10^9	0.25	3500	6100

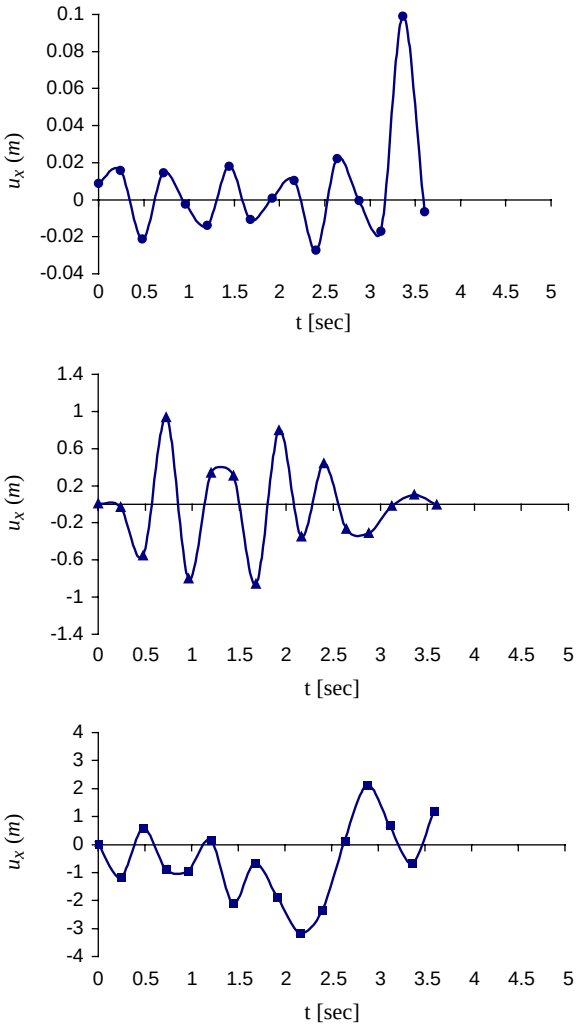

Fig. 7. Transient displacement u_x at T_3 (90, 0) on the free surface for P-wave $(\sin(pt), p = 10)$ with incidence angle $\alpha = 0^\circ$ at the half-space boundary: Case •, no cracks; Case ▲, an interface crack; Case ■, both types of cracks.

those of Ref. [40] at the $\beta = 0.01$ level. It is observed that the new results are very close, but the best overall agreement is still observed in Fig. 6a.

6. Transient scattering of seismic waves by cracks in a multi-layered geological deposit

The geometry and mechanical properties of the geological deposit whose seismic behaviour is examined here are shown in Fig. 1 and Table 1, respectively. In addition, surface topography Ω_4 comprises a circular cylindrical canyon with radius $A = 30$ m. The region is being swept by P-waves that trace incident angles with respect to the vertical of $\alpha = 0^\circ, \alpha = 30^\circ$ and $\alpha = 85^\circ$. The

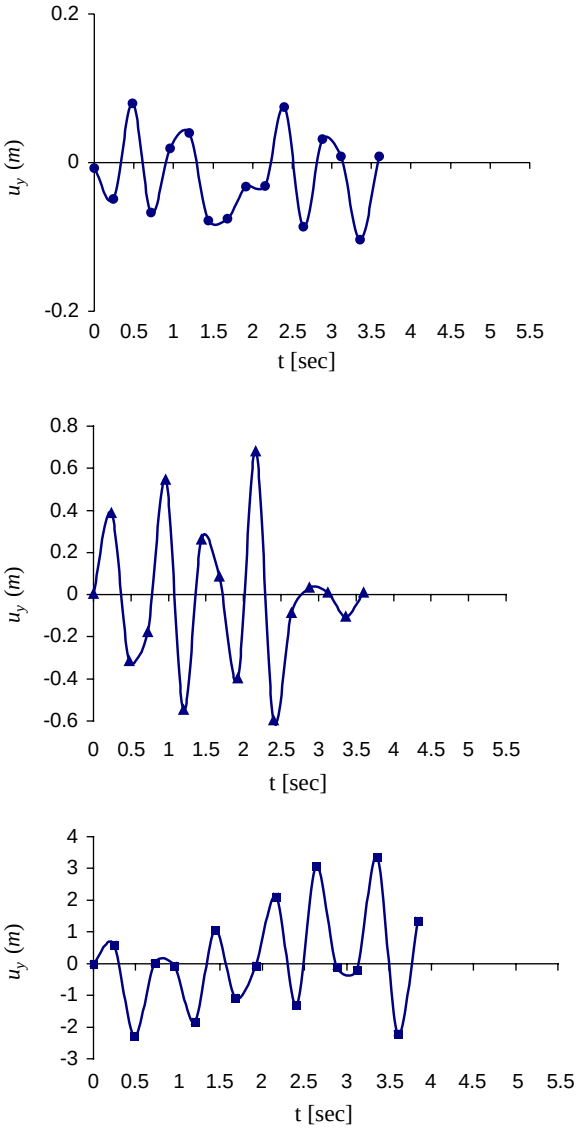

Fig. 8. Transient displacement u_y at T_3 (90, 0) on the free surface for P-wave $(\sin(pt), p = 10)$ with incidence angle $\alpha = 0^\circ$ at the half-space boundary: Case •, no cracks; Case ▲, an interface crack; Case ■, both types of cracks.

time variation of the P-waves is harmonic and given as $f(t) = \sin pt$, where frequency $p = 10$ rad/s, while the duration of the dynamic event is $T = 4.8$ s. Finally, the basic numerical Laplace transform inversion parameters are $T = 5.0$ s, $b = 6.0/T$ and $N = 50$.

6.1. Computation of synthetic seismograms

Two sub-cases are distinguished with respect to the geological deposit of Fig. 1, namely (i) the presence of a single interface crack EF of length $l_{ifc} = 75$ m with endpoint co-ordinates

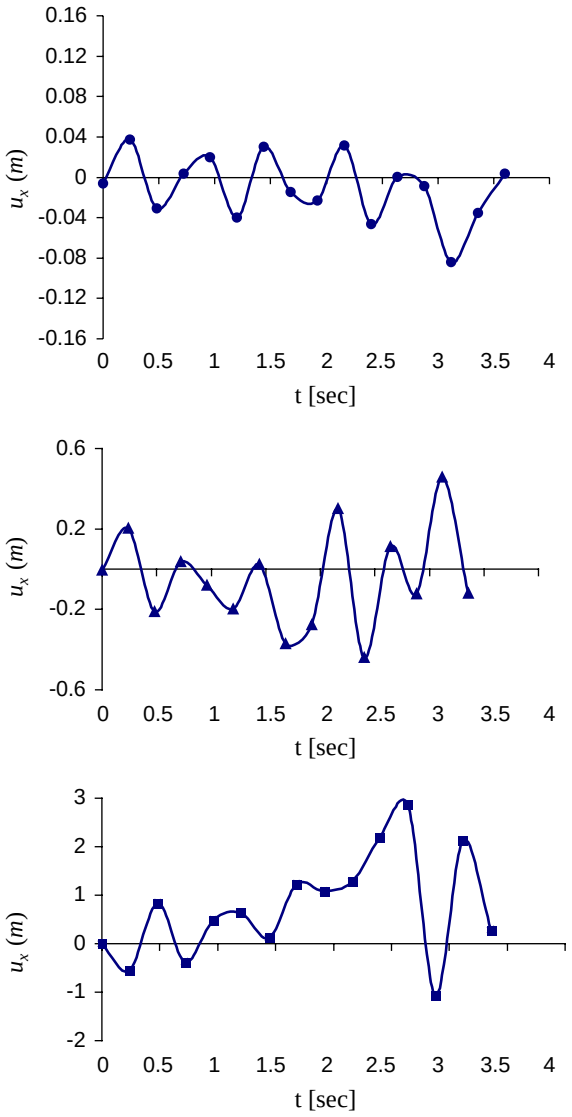

Fig. 9. Transient displacement u_x at mid-point (45, 0) of T_1T_2 on the free surface for P-wave $(\sin(pt), p = 10)$ with incidence angle $\alpha = 0^\circ$ at the half-space boundary: Case •, no cracks; Case ▲, an interface crack; Case ■, both types of cracks.

$F(45, 90), E(-30, 90)$ and (ii) the presence of two cracks, namely the previous interface crack plus an internal crack MN inside layer Ω_2 of length $l_{ifc} = 120$ m and endpoint co-ordinates $M(60, 120), N(-60, 120)$. In both sub-cases, the deposit rests on bedrock that has wave speeds of $C_S = 3500$ m/s and $C_P = 6100$ m/s. Finally, the amplitude of the transient incident wave is conveniently taken as $u_{0x} = 0.0$ mm, $u_{0y} = 0.1$ mm.

The problem has been solved by the methodology developed in the previous sections and all results are summarized in Figs. 7–20, from which the influence of factors such as surface

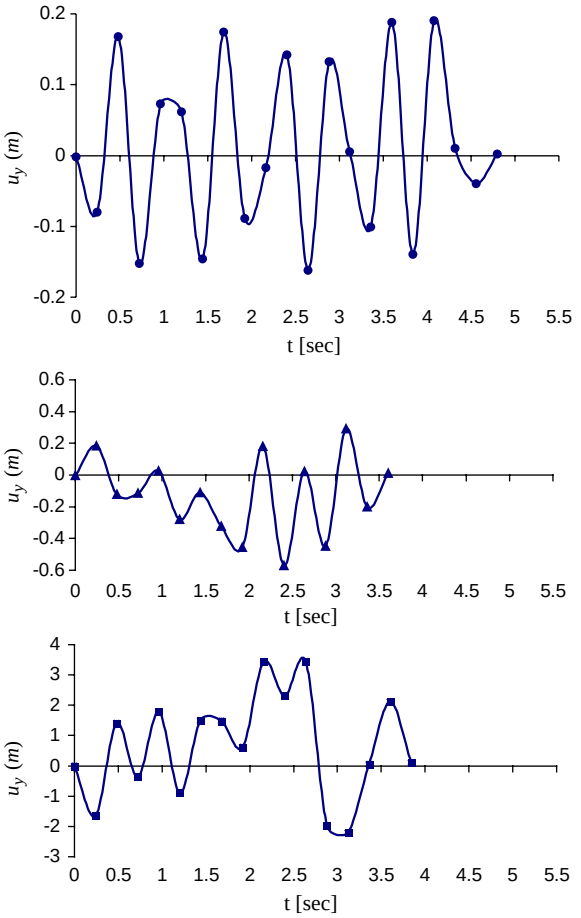

Fig. 10. Transient displacement u_y at mid-point (45, 0) of T_1T_2 on the free surface for P-wave ($\sin(pt), p = 10$) with incidence angle $\alpha = 0^\circ$ at the half-space boundary: Case •, no cracks; Case ▲, an interface crack; Case ■, both types of cracks.

topography, P-wave incidence angle and crack interaction on the scattered displacement field that develops at the free surface can be surmised. All these effects are discussed separately below.

(*a*) *The effect of surface topography*: Surface topography influence on ground motions (synthetic seismograms) is investigated at three different locations on the free surface, namely point $T_3 = (90, 0)$, at the midpoint of segment T_1T_2 with co-ordinates $(45, 0)$ and at a point on arc segment P_1T_1 along the canyon surface with co-ordinates (21.2, 21.2). These motions are for the incident P-wave with harmonic time variation impinging on boundary LL_1 under incident angle $\alpha = 0^\circ$ and are collected in Figs. 7–12. Furthermore, Figs. 13–18 plot the same type of information, but for an incident angle $\alpha = 85^\circ$, which is a nearly horizontal sweep. In all cases, dividing with the value of the incident wave amplitude normalizes the scattered displacement field. Throughout these plots, the topography effect can be discerned by contrasting three different

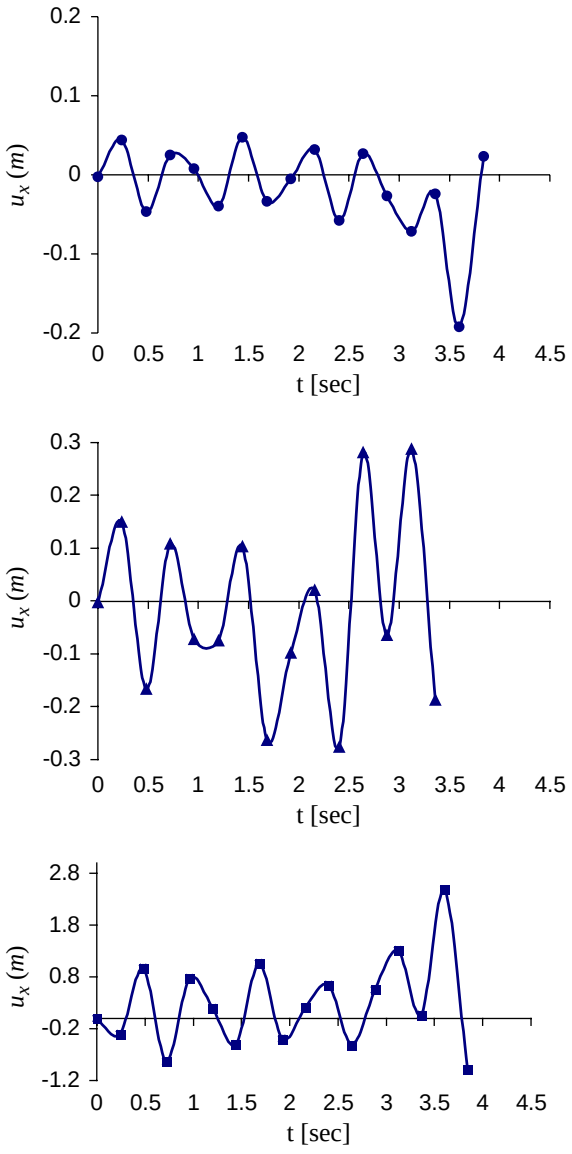

Fig. 11. Transient displacement u_x at point $(21.2, 21.2) \in P_1T_1$ on the free surface for P-wave $(\sin(pt), p = 10)$ with incidence angle $\alpha = 0^\circ$ at the half-space boundary: Case ●, no cracks; Case ▲, an interface crack; Case ■, both types of cracks.

situations, namely (i) the canyon is in the uncracked, finite layered region; (ii) the canyon is inside the layered region with interface crack $EF$and (iii) the canyon is inside the layered region in the presence of both interface crack EF and internal crack MN in layer Ω_2. As expected, the wave scattering picture that emerges is complex and differences can be observed between all three cases. Specifically, a comparison of Figs. 7, 9 and 11 shows that the maximum horizontal displacements

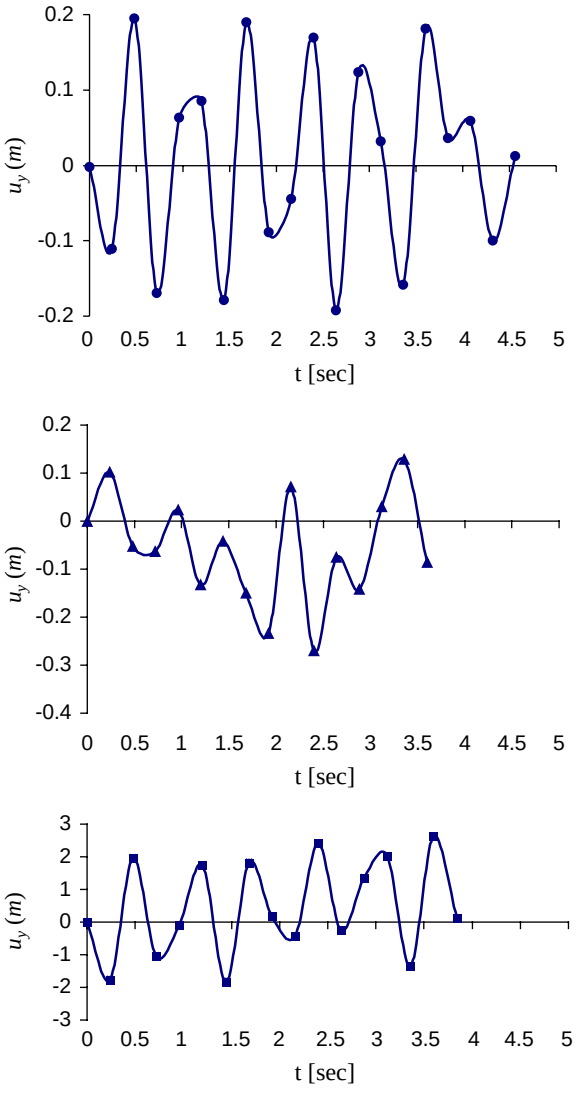

Fig. 12. Transient displacement u_y at point $(21.2, 21.2) \in P_1T_1$ on the free surface for P-wave $(\sin(pt), p = 10)$ with incidence angle $\alpha = 0^\circ$ at the half-space boundary: Case •, no cracks; Case ▲, an interface crack; Case ■, both types of cracks.

recorded along the surface of the canyon in the absence of cracks are somewhat larger (0.2 versus 0.1) compared to the other free surface locations. A roughly similar picture emerges for the vertical displacements by consulting Figs. 8, 10 and 12. For an angle of wave incidence close to the horizontal, there is little difference in the amplitude values recorded for the horizontal displacements (all are around 0.1); the vertical displacements are roughly half that value, or even less.

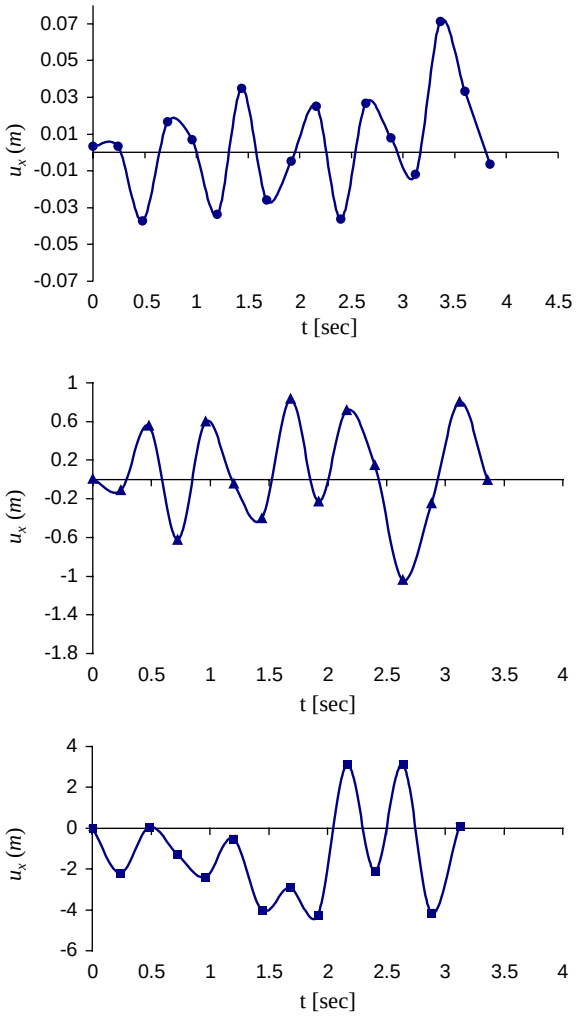

Fig. 13. Transient displacement u_x at point T_3 $(90, 0)$ on the free surface for P-wave $(\sin(pt), p = 10)$ with incidence angle $\alpha = 85^\circ$ at the half-space boundary: Case •, no cracks; Case ▲, an interface crack; Case ■, both types of cracks.

(*b*) *The effect of a single crack*: This effect is clearly manifested in all figures as the incident wave propagates along the vertical direction. Specifically, they all show a significant increase in the scattered displacement field amplitude in the presence of a crack, independently of the location of the receivers. This increase is of an order of magnitude for receivers on the horizontal free surface (e.g., from 0.1 to 1.0), but much less for receivers along the canyon walls (e.g., from 0.2 to 0.3), irrespective of the type of displacement component (horizontal versus vertical). When the angle of wave incidence is close to the horizontal, the aforementioned amplification phenomenon is less. This can be explained by the fact that points which fall into the shadow zone behind the interface crack are screened by the crack itself.

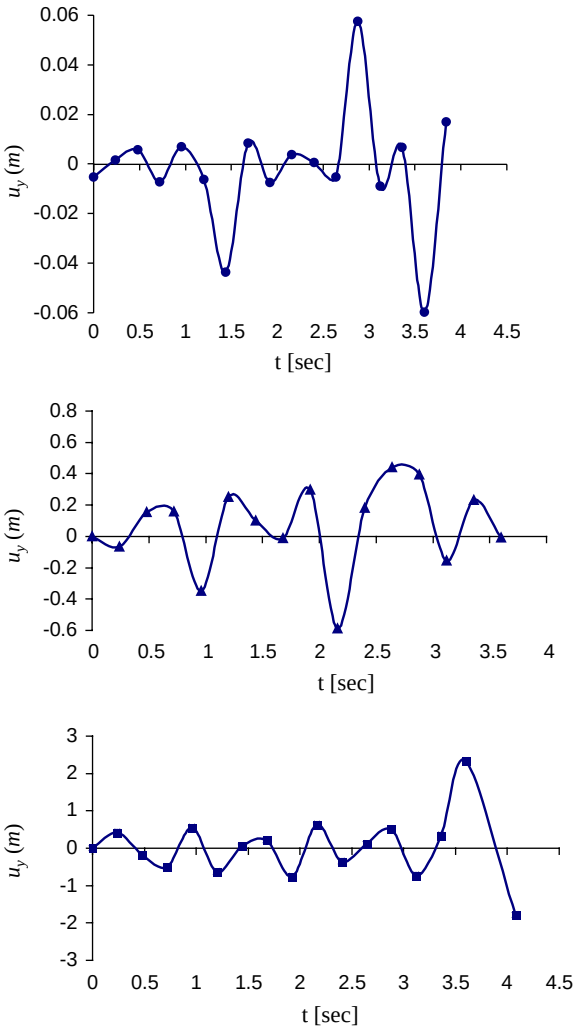

Fig. 14. Transient displacement u_y at point T_3 $(90, 0)$ on the free surface for P-wave $(\sin(pt), p = 10)$ with incidence angle $\alpha = 85^\circ$ at the half-space boundary: Case •, no cracks; Case ▲, an interface crack; Case ■, both types of cracks.

(*c*) *The crack interaction effect*: Comparing the single crack case with the combined interface/internal crack case identifies the crack interaction effect. Again, all figures clearly depict the increase in displacements along the free surface when there are two interacting cracks in the geological region. This increase is dependent on the angle of wave incidence and on the location of the receiver point, with the most pronounced situation (a quadrupling) registering at T_3 and for $\alpha = 85^\circ$, followed by the T_3 and $\alpha = 0^\circ$ combination (a doubling). Finally, all the above figures show the complex interaction picture that develops as the seismic waves are scattered by the canyon relief and the crack-tips, reflected at the boundaries of the layers and transmitted through the interfaces where material properties are discontinuous.

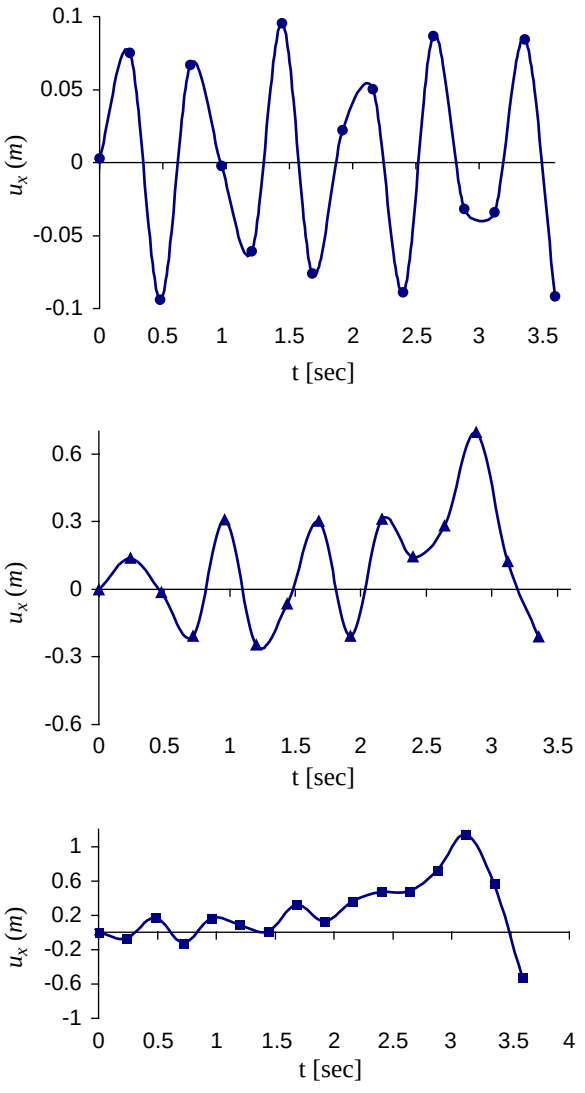

Fig. 15. Transient displacement u_x at mid-point (45, 0) of T_1T_2 on the free surface for P-wave ($\sin(pt), p = 10$) with incidence angle $\alpha = 85^\circ$ at the half-space boundary: Case •, no cracks; Case ▲, an interface crack; Case ■, both types of cracks.

6.2. *Evaluation of the transient stress concentration field near an interface crack*

The aim of this section is to investigate the near crack-tip stress concentration field. The overall SIF K_0^{right} is obtained from Eq. (16) using COD at the right crack-tips versus time and is given in Figs. 19 and 20. This SIF is normalized by $\mu\sqrt{\pi l_{int}}$, where l_{int} is the length of the right QP-BE. More specifically, Fig. 19 presents the dynamic stress concentration field near the interface crack

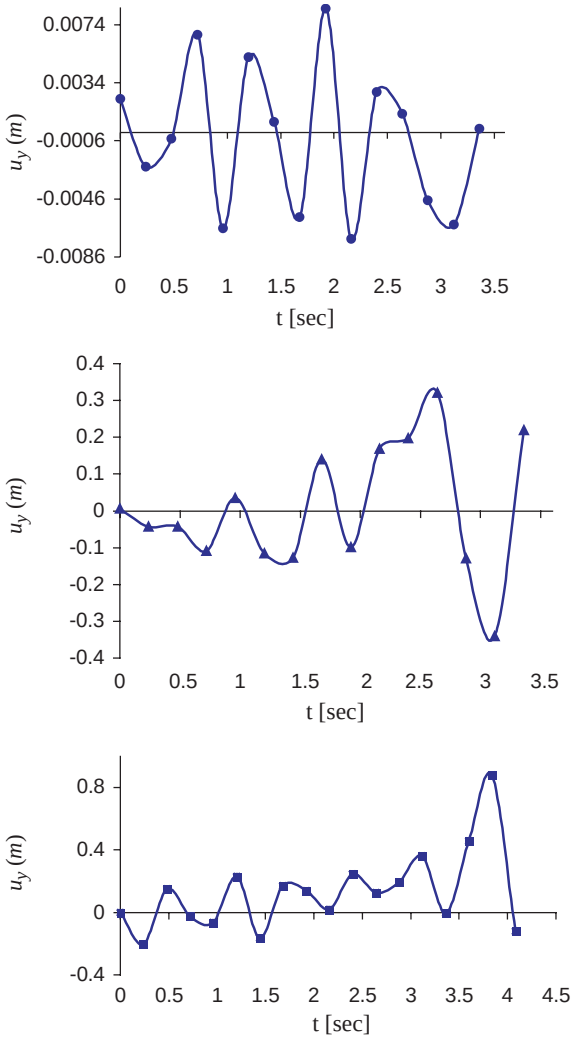

Fig. 16. Transient displacement u_y at mid-point (45, 0) of T_1T_2 on the free surface for P-wave ($\sin(pt), p = 10$) with incidence angle $\alpha = 85^\circ$ at the half-space boundary: Case ●, no cracks; Case ▲, an interface crack; Case ■, both types of cracks.

under the incident transient P-wave in the presence of a single crack, while Fig. 20 plots the same picture when both internal and interface cracks are present. In all cases, the maximum value of the SIF curves occurs after time $t = 2.4$ s. As far as the influence of the incidence angle is concerned, the SIF values are greater when $\alpha = 0^\circ$ as compared to $\alpha = 85^\circ$, with $\alpha = 30^\circ$ being an intermediate situation. Finally, the crack interaction effect is clearly manifested when contrasting Figs. 19 and 20 and observing that the SIF at the interface crack-tip is almost an order of magnitude greater in the presence of an additional internal crack in the geological region. For the single crack case, the maximum SIF drops from 1.4 to 0.4 as the incoming wave shifts from a

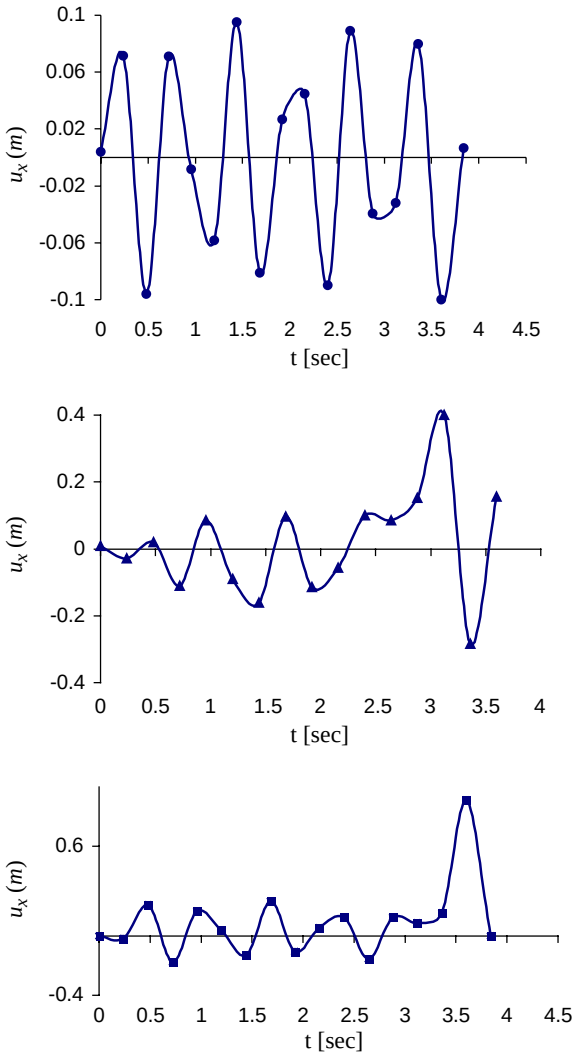

Fig. 17. Transient displacement u_x at point $(21.2, 21.2) \in P_1T_1$ on the free surface for P-wave $(\sin(pt), p = 10)$ with incidence angle $\alpha = 85^\circ$ at the half-space boundary: Case •, no cracks; Case ▲, an interface crack; Case ■, both types of cracks.

vertical to a nearly horizontal orientation, while for the interacting crack case, the corresponding SIF drop is from 6.5 to 3.0.

7. Conclusions

In this work, a numerical model is developed for seismic wave propagation in multi-layered, cracked geological deposits with topographic relief at the free surface. More specifically, transient

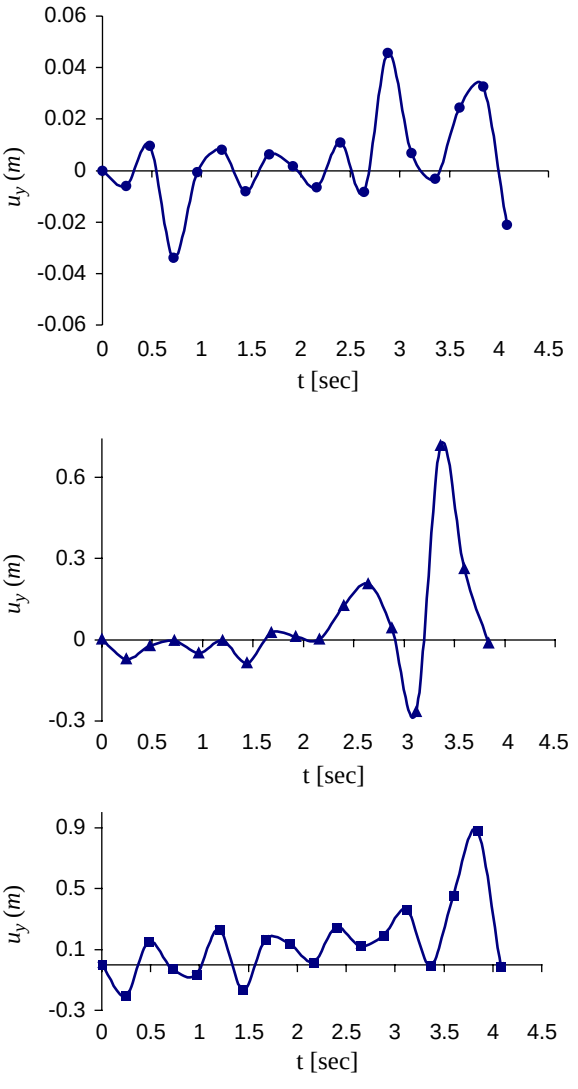

Fig. 18. Transient displacement u_y at point $(21.2, 21.2) \in P_1T_1$ on the free surface for P-wave $(\sin(pt), p = 10)$ with incidence angle $\alpha = 85^\circ$ at the half-space boundary: Case ●, no cracks; Case ▲, an interface crack; Case ■, both types of cracks.

conditions were assumed to hold, while both interface and internal cracks are present in the geological continuum. By assuming plane strain conditions, this elastic wave scattering problem is solved by introducing a combined displacement and regularized traction BIE in the Laplace transformed domain. Although the basic strategy, which calls for superposition of crack-free and cracked states along with a breakdown of the problem into multiple regions, is well known in fracture mechanics, the present contribution is in using these types of numerical tools for solving 2D wave scattering problems in complex geological regions. The transient nature of the scattered

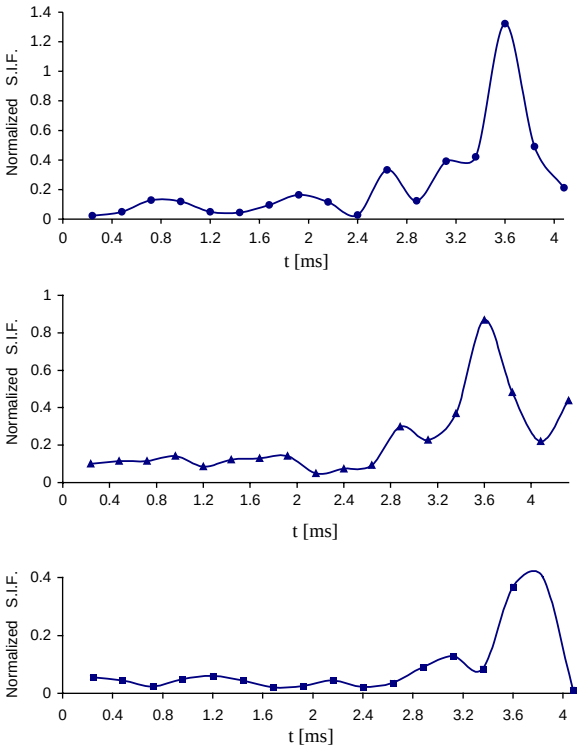

Fig. 19. Normalized transient SIF K_0^{right} due to incident P-wave ($\sin(pt), p = 10$) at the half-space boundary of the multi-layered region and for a single interface crack: Case •, incidence angle $\alpha = 0°$; Case ▲, incidence angle $\alpha = 30°$; Case ■, incidence angle $\alpha = 85°$.

wave fields is subsequently reconstituted through use of a numerical inverse Laplace transformation. As far as spatial discretization is concerned, parabolic-type boundary elements are employed, supplemented by special crack-tip elements in the vicinity of the cracks. The types of numerical results that are obtained herein are synthetic seismograms at receivers on the free surface of the geological deposit and SIF near the crack-tips. In all cases, the results produced by the present methodology show that both scattered wave displacement field on the free surface and stress concentration field near the crack-tips are sensitive to site conditions such as the existence of surface relief, the presence of layers and cracks, and most importantly on interaction effects due to the presence of multiple cracks. In sum, this type of work is useful in the field of earthquake engineering, where a detailed image of local ground motions is of paramount importance.

Acknowledgements

The authors wish to acknowledge the financial support provided under NATO grant No. EST.CLG. 977774.

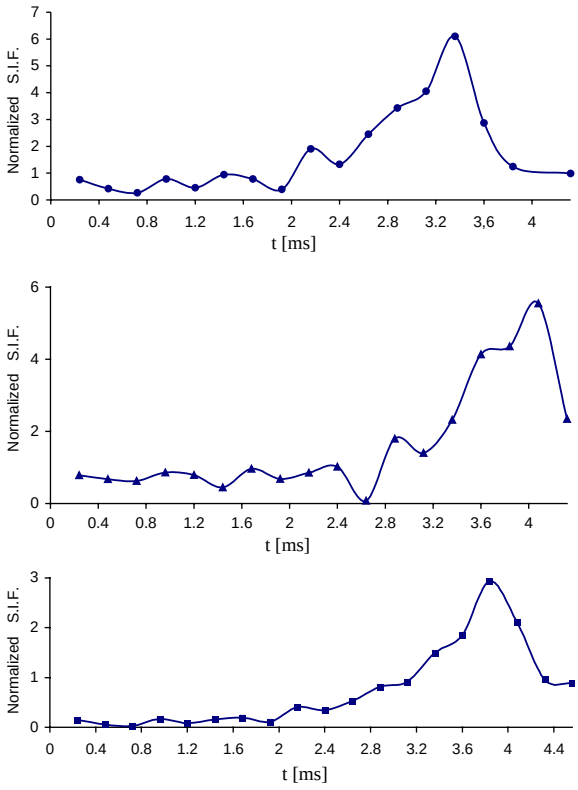

Fig. 20. Normalized transient SIF K_0^{right} due to incident P-wave $(\sin(pt), p = 10)$ at the half-space boundary of the multi-layered region for both interface and internal cracks: Case •, incidence angle $\alpha = 0°$; Case ▲, incidence angle $\alpha = 30°$; Case ■, incidence angle $\alpha = 85°$.

References

[1] M.D. Trifunac, Surface motion of a semi-cylindrical alluvial valley for incident plane SH waves, *Bulletin of Seismology Society of America* 61 (1971) 1755–1770.
[2] H.L. Wong, M.D. Trifunac, Surface motion of a semi-elliptical alluvial valley for incident plane SH-waves, *Bulletin of Seismology Society of America* 64 (1974) 1389–1403.
[3] F.J. Sanchez-Sesma, Diffraction of elastic waves by three dimensional surface irregularities, *Bulletin of Seismology Society of America* 73 (1983) 1621–1636.
[4] N. Moen-Vaziri, M.D. Trifunac, Scattering and diffraction of plane P- and SV-waves by two-dimensional inhomogeneities: Part II, *Soil Dynamics and Earthquake Engineering* 7 (1988) 189–200.
[5] V.W. Lee, X. Wu, Application of the weighted residual method to diffraction by 2-D canyons of arbitrary shape: II. Incident P, SV, and Rayleigh waves, *Soil Dynamics and Earthquake Engineering* 13 (1994) 365–375.
[6] V. Cerveny, R. Ravindra, *Theory of Seismic Head Waves*, University of Toronto Press, Toronto, 1971.
[7] T.L. Houg, D.V. Helmberger, Glorified optics and wave propagation in non-linear structure, *Bulletin of Seismology Society of America* 68 (1978) 1313–1330.
[8] J.J. Lee, C.A. Langston, Wave propagation in a three dimensional circular basin, *Bulletin of Seismology Society of America* 73 (1983) 1637–1653.
[9] P. Moczo, P.Y. Bard, I. Psencik, Seismic response of two-dimensional absorbing structures by the ray method, *Journal of Geophysics* 62 (1987) 38–49.

[10] G. Waas, Linear Two-Dimensional Analysis of Soil Dynamic Problems in Semi-Infinite Layered Media, PhD Dissertation, University of California, Berkeley, CA, 1972.
[11] J. Lysmer, T. Udaka, H.B. Seed, R. Hwang, LUSH, a computer program for complex response analysis of soil-structure systems. Report No. EERC 74-4, Earthquake Engineering Research Center, University of California, Berkeley, CA, 1974.
[12] E. Kausel, Forced vibrations of circular foundations in layered media, MIT Research Report No. 74-11, Department of Civil Engineering, Massachusetts Institute of Technology, Cambridge, MA, 1974.
[13] K. Aki, K.L. Larner, Surface motion of a layered medium having an irregular interface due to incident plane SH-waves, *Journal of Geophysical Research* 75 (1970) 933–954.
[14] M. Bouchon, M. Campillo, S. Gaffet, A boundary integral equation-discrete wave number representation method to study wave propagation in multi-layered media having irregular interfaces, *Geophysics* 54 (1989) 1134–1140.
[15] D.M. Boore, Finite difference method for seismic wave propagation in heterogeneous materials, in: D.M. Boore (Ed.), *Methods in Computational Physics*, Vol. 11, Academic Press, New York, 1972, pp. 1–37.
[16] G. Nolet, R. Sleeman, V. Nijhof, B.L.N. Kennett, Synthetic reflection seismograms in three dimensions by a locked mode approximation, *Geophysics* 54 (1989) 1134–1140.
[17] H.A. Pedersen, F.J. Sanchez-Sesma, M. Campillo, Three-dimensional scattering by two-dimensional topographies, *Bulletin of Seismology Society of America* 84 (1994) 1169–1183.
[18] F.J. Sanchez-Sesma, R. Vai, E. Dretta, V.J. Palencia, Fundamentals of elastic wave propagation for site amplification studies: the seismic response of alluvial valleys, in: E. Kausel, G.D. Manolis (Eds.), *Wave Motion Problems in Earthquake Engineering*, WIT Press, Southampton, Chapter 1.
[19] M. Bouchon, C.A. Schultz, M.N. Toksoz, A fast implementation of boundary integral equation methods to calculate the propagation of seismic waves in laterally varying layered media, *Bulletin of Seismology Society of America* 85 (1995) 1679–1687.
[20] T. Yokoi, H. Takenaka, Treatment of an infinitely extended free surface for indirect formulation of the boundary element method, *Journal on Physics of Earth* 43 (1995) 79–103.
[21] R. Vai, J.M. Castillo-Covarrubias, F.J. Sanchez-Sesma, D. Komatitsh, J.P. Violotte, Elastic wave propagation in an irregularly layered medium, *Soil Dynamic and Earthquake Engineering* 18 (1999) 11–18.
[22] P.Y. Bard, M. Bouchon, The seismic response of sediment-filled valleys. Part 1: the case of incident SH waves, *Bulletin of Seismology Society of America* 70 (1980) 1263–1286.
[23] P.Y. Bard, M. Bouchon, The seismic response of sediment-filled valleys. Part 2: the case of incident P- and SV- waves, *Bulletin of Seismology Society of America* 70 (1980) 1921–1941.
[24] P.Y. Bard, M. Bouchon, The two-dimensional resonance of sediment-filled valleys, *Bulletin of Seismology Society of America* 75 (1980) 519–541.
[25] H. Eshrachi, M. Dravinski, Transient scattering of elastic waves by dipping layers of arbitrary shape. Part 1: anti-plane strain model, *Earthquake Engineering and Structural Dynamics* 18 (1989) 397–415.
[26] H. Eshrachi, M. Dravinski, Transient scattering of elastic waves by dipping layers of arbitrary shape. Part 2: plane strain model, *Earthquake Engineering and Structural Dynamics* 18 (1989) 417–434.
[27] A.H. Shah, K.G. Wong, S.K. Datta, Diffraction of plane SH waves in a half-space, *Earthquake Engineering and Structural Dynamics* 10 (1982) 519–528.
[28] T. Furumura, K. Koketsu, K. Wen, Parallel PSM/FDM hybrid simulation of ground motions from the 1999 Chi-Chi Taiwan earthquake, *Pure and Applied Geophysics* 159 (2002) 2133–2146.
[29] G.F. Panza, F. Romanelli, F. Vaccari, Seismic wave propagation in laterally heterogeneous anelastic media: theory and applications to seismic zonation, *Advances in Geophysics* 43 (2000) 1–95.
[30] Y. Niwa, S. Hirose, Application of the BEM to elastodynamics in a 3D half-space, in: D.L. Karabalis (Ed.), *Recent Applications in Computational Mechanics*, ASCE, New York, 1986, pp. 1–15.
[31] G.D. Manolis, D.E. Beskos, *Boundary Element Methods in Elastodynamics*, Allen and Unwin, London, 1987.
[32] D.E. Beskos, Boundary element methods in dynamic analysis: Part II (1986–1996), *Applied Mechanics Reviews* 50 (1997) 149–197.
[33] R. Gallego, J. Dominguez, Dynamic crack propagation analysis by moving singular boundary elements, *Journal of Applied Mechanics* 59 (1992) S158–S162.

[34] A.S.M. Israil, P.K. Banerjee, Two-dimensional transient wave-propagation problems by time-domain BEM, *International Journal of Solids and Structures* 26 (1990) 851–864.
[35] W.J. Mansur, C.A. Brebbia, Transient elastodynamics, in: C.A. Brebbia (Ed.), *Topics in Boundary Elements Research*, Springer, Berlin, 1985.
[36] T.A. Cruse, F.J. Rizzo, A direct formulation and numerical solution of the general transient elastodynamic problem, Part I, *International Journal of Mathematical Analysis and Applications* 22 (1968) 244–259.
[37] T.A. Cruse, A direct formulation and numerical solution of the general transient elastodynamic problem, Part II, *International Journal of Mathematical Analysis and Applications* 22 (1968) 341–355.
[38] G.D. Manolis, D.E. Beskos, Dynamic stress concentration studies by boundary integrals and Laplace transform, *International Journal of Numerical Methods in Engineering* 17 (1981) 573–599.
[39] V. Sladek, J. Sladek, Transient elastodynamic three-dimensional problems in cracked bodies, *Applied Mathematical Modelling* 8 (1984) 2–10.
[40] F. Chirino, J. Dominguez, Dynamic analysis of cracks using BEM, *Engineering Fracture Mechanics* 34 (1989) 1051–1061.
[41] A. Portela, M.H. Aliabadi, D.P. Rooke, The dual boundary element method: effective implementation for crack problems, *International Journal of Numerical Methods in Engineering* 33 (1992) 1269–1287.
[42] P. Fedelinski, M.H. Aliabadi, D.P. Rooke, Boundary element formulations for the dynamic analysis of cracked structures, *Engineering Analysis with Boundary Elements* 17 (1996) 45–56.
[43] K. Yomogida, R. Benites, Scattering of seismic waves by cracks with boundary integral method, *Pure and Applied Geophysics* 159 (2002) 1771–1789.
[44] J. Chen, H.K. Hong, Review of dual boundary element methods with emphasis on hypersingular integrals and divergent series, *Applied Mechanics Reviews* 52 (1999) 17–33.
[45] D. Nardini, C.A. Brebbia, A new approach to free vibration analysis using boundary elements, in: C.A. Brebbia, (Ed.), *BEM in Engineering*, Springer, Berlin, 1982.
[46] J. Dominguez, *Boundary Elements in Dynamics*, Computational Mechanics Publications, Southampton, 1993.
[47] P.S. Dineva, P. Borejko, L. Hadjikov, F. Ziegler, Transient elastic waves in a half-space: comparison of the DBIE-method with the method of generalized ray, *Acta Mechanica* 115 (1996) 203–211.
[48] P.S. Dineva, E. Gavrilova, Waves propagation in a multi-layered geological region. Part II: transient case, *International Journal of Seismology and Earthquake Engineering* 2 (2000) 1–8.
[49] K. Aki, P. Richards, *Quantitative Seismology: Theory and Methods*, W.H. Freeman, San Francisco, 1980.
[50] A. Zerva, Spatial variability of seismic motions recorded over extended ground surface areas, in: E. Kausel. G.D. Manolis (Eds.), *Wave Motion Problems in Earthquake Engineering*, WIT Press, Southampton, 2001 (Chapter 3).
[51] P.S. Dineva, G.D. Manolis, Scattering of seismic waves by cracks in multi-layered geological regions: I. Mechanical model, *Soil Dynamics and Earthquake Engineering* 21 (2001) 615–625.
[52] P.S. Dineva, G.D. Manolis, Scattering of seismic waves by cracks in multi-layered geological regions: II. Numerical results, *Soil Dynamics and Earthquake Engineering* 21 (2001) 627–641.
[53] G.E. Blandford, A.R. Ingrafea, J.A. Ligget, Two-dimensional stress intensity factor computations using the boundary element method, *International Journal for Numerical Methods in Engineering* 17 (1981) 387–404.
[54] J. Sladek, V. Sladek, Dynamic SIF studied by boundary integro-differential equations, *International Journal for Numerical Methods in Engineering* 23 (1986) 919–928.
[55] T.V. Rangelov, P.S. Dineva, Numerical solution of integro-differential equations for a finite elastic cracked bodies, *Comptes Rendus de l'Academie Bulgare des Sciences* 53 (9) (2000) 31–34.
[56] T. Rangelov, P. Dineva, D. Gross, A hypersingular traction boundary integral equation method for stress intensity factor computation in a finite cracked body, *Engineering Analysis with Boundary Elements* 27 (2003) 9–21.
[57] M.H. Aliabadi, D.P. Rooke, *Numerical Fracture Mechanics*, Computational Mechanics Publications, Southampton, 1991.
[58] C. Zhang, D. Gross, *Wave Propagation in Elastic Solids with Cracks*, Computational Mechanics Publications, Southampton, 1988.
[59] F. Durbin, Numerical inversion of Laplace transform: an efficient improvement to Dubner and Abate's method, *Computation Journal* 17 (1974) 297–301.

[60] P. Duhamel, M. Vetterling, Fast Fourier transform: a tutorial review and a state of the art, *Signal Processing* 19 (1990) 259–299.
[61] G.D. Manolis, P.S. Dineva, T.V. Rangelov, Seismic waves propagating in a cracked multi-layered geological region, Research Report for NATO grant EST.CLG. 977774, Department of Civil Engineering, Aristotle University, Thessaloniki, Greece, 2002.
[62] Y.M. Chen, Numerical computation of dynamic SIF by Lagrangian finite-difference method, *Engineering Fracture Mechanics* 7 (1975) 653–660.
[63] V. Murti, S. Valliappan, The use of quarter point element in dynamic crack analysis, *Engineering Fracture Mechanics* 23 (1986) 585–614.
[64] Y. Jiaju, J. Xing, Numerical computation of dynamic SIF by the BEM, *Engineering Analysis with Boundary Elements* 5 (1988) 140–145.